Taylor & Francis
Taylor & Francis Group

ORIGINAL RESEARCH

🔓 OPEN ACCESS | Check for updates

Pirfenidone facilitates immune infiltration and enhances the antitumor efficacy of PD-L1 blockade in mice

Wan Qin[a#], Jun Zou[a#], Yongbiao Huang[a], Chaofan Liu[a], Yalin Kang[a], Hu Han[a,b], Yang Tang[a], Long Li[a], Bo Liu[a], Weiheng Zhao[a], and Xianglin Yuan[a]

[a]Department of Oncology, Tongji Hospital, Huazhong University of Science and Technology, Wuhan, Hubei, China; [b]Department of Oncology, First Affiliated Hospital, Shihezi University, Shihezi, Xinjiang, China

ABSTRACT

Idiopathic pulmonary fibrosis (IPF) patients have a high risk of developing lung cancer, with few treatment options available. Pirfenidone, an antifibrotic agent approved for the treatment of IPF, has been demonstrated to suppress the TGFβ signaling and modulate the expression of immune-related genes. However, for lung cancer patients with comorbid IPF, whether pirfenidone has any synergetic effect with immune checkpoint inhibitors has not been investigated. In this study, we showed that pirfenidone monotherapy attenuated tumor growth with an increased T cell inflammatory signature in tumors. Co-administration of pirfenidone with PD-L1 blockades significantly delayed the tumor growth and increased survival, compared with the effect of either treatment alone. Combination therapy promoted gene expression with a unique signature associated with innate and adaptive immune response resulted in the infiltration of immune cells and optimal T cell positioning. Furthermore, we showed a great benefit of combination therapy in alleviating the pulmonary fibrosis and reducing the tumor growth in a tumor-fibrosis model. Our results collectively demonstrated that pirfenidone facilitated antitumor immunity and enhanced the efficacy of PD-L1 blockades. It may act as an adjuvant to immunotherapy in cancer treatment, particularly, in lung cancer patients with preexisting IPF.

Introduction

Idiopathic pulmonary fibrosis (IPF) is a chronic, progressive, and fatal disease that is characterized by irreversible scarring of the lung.[1] Although the underlying mechanisms are not fully understood, IPF is associated with an increased risk of lung cancer, ranging from 9.8% to over 50% depending on observation period.[2] Both diseases present with major similarities in terms of pathogenetic pathways, as well as potential causative factors, such as smoking and viral infections.[3] Lung cancer patients with comorbid IPF have few treatment options because surgery, radiotherapy, and chemotherapy elevate the risk of exacerbation of IPF.[4–6]An optimal therapeutic strategy for patients with both diseases is sorely needed.

Pirfenidone (PFD) is a small pyridine compound synthesized by Morgolin in 1974 and approved for the treatment of mild to moderate IPF in 2011 and 2014 in Europe and the United States, respectively.[7] Although the exact mechanism of action is not fully understood, studies conducted by us[8] as well as others[9] suggest that PFD exerts dramatic antifibrotic properties through downregulating TGFβ signaling, reducing fibroblast proliferation, and inhibiting collagen synthesis. Recently, a study using transcriptomic approach revealed that in IPF patients, genes altered by PFD are enriched not only in "extracellular matrix," but also in "immune response."[10] PFD reduced immune-suppressive capacity of cancer-associated

fibroblasts (CAF) by modulating various cytokines in CAF in vitro.[11] In addition, PFD controlled tumor growth and increase the infiltration of T cells and NK cells in a murine tumor model.[12] Therefore, PFD may have effect on immune microenvironment regardless of antifibrotic properties.

Immune checkpoint inhibitors (ICIs) that block the programmed death-1 (PD-1)/programmed death-ligand 1 (PD-L1) interaction can induce robust and durable responses and have dramatically altered the treatment landscape of non-small cell lung cancer (NSCLC).[13] However, most patients do not benefit from this treatment owing to primary resistance. How to extend the clinical benefits to the majority of patients with cancer have been key focuses of this area. Several types of tumors display an "immune excluded" phenotype, in which T cells are restricted to a peritumoral zone that is rich in fibroblasts.[14] These tumors are immunologically cold tumors that respond poorly to ICIs. Recently, TGFβ signaling has been identified to play a key role in T cell exclusion in the tumor microenvironment.[15,16] Combining ICIs with TGFβ inhibitors such as antibodies,[16] chemicals,[17] and bifunctional fusion proteins[18] has been shown to induce complete and durable responses in poorly immunogenic tumors.

For lung cancer patients with comorbid IPF, whether concurrently taking PFD has an influence on the antitumor efficacy of ICIs is unknown. As PFD has the ability to suppress the

---

[#]These authors contribute equally to this work.
ⓘ Supplemental data for this article can be accessed on the publisher's website.

TGFβ signaling, we hypothesized that it may have the capacity to enhance the antitumor efficacy of ICIs. In the current study, we used syngeneic tumor mouse models to evaluate the efficacy of PFD combined with PD-L1 blockades. RNA sequencing, flow cytometry and immunohistochemistry were conducted to elucidate the underlying mechanisms.

Materials and methods

Mice, cell lines, and reagents

All procedures were approved by the Institutional Animal Care and Use Committee of Tongji Medical College, Huazhong University of Science and Technology (approval number: TJ-A20180505).

Female C57BL/6 mice, BALB/c mice and BALB/c nude mice (6 to 8 weeks of age) were obtained from the Experimental Animal Center of Hubei Province, housed 6 per cage under standard laboratory conditions and fed with sterilized food and water *ad libitum*.

The lung cancer cell lines A549 and H292, Lewis lung cancer (LLC) cell line, and H22 hepatocellular carcinoma cell line were obtained from the China Center for Type Culture Collection. The MC38 cell line was obtained from the Research Center for Tissue Engineering and Regenerative Medicine, Union Hospital, Tongji Medical College, Huazhong University of Science and Technology. The LLC luciferase positive (LLC-luc) cell line was developed from the LLC parental cell line stably transduced with firefly luciferase (luciferase plasmid pLXSN-luc, G418). All cell lines were validated to be mycoplasma-free. All mouse-derived cell lines (LLC-luc, MC38, H22) were tested for in vivo tumor formation in immunocompetent mice in our preliminary experiment.

PFD was kindly provided by Beijing Continent Pharmaceutical Co., Ltd. (Beijing, China). Anti-PD-L1 antibody (clone 10 F.9G2, Cat#BE0101) was purchased from BioXcell (West Lebanon, NH, USA). Galunisertib (Cat#HY-13226) and bleomycin sulfate (Cat#HY-17565) were purchased from MedChem Express (MonmouthJunction, New Jersey, USA).

Animal model generation and treatment

LLC-luc or MC38 tumors were generated by the subcutaneous injection of 1×10^6 cells into the flank of C57BL/6 or athymic nude mice. For H22 tumors generation, 1×10^7 cells were injected into the peritoneal cavities of BALB/C mice. The viscous ascites was extracted and 1×10^6 ascites tumor cells were injected into the flank of BALB/C mice 7–9 d later.

PFD was administered orally at 500 mg/kg once every day. Galunisertib was administered orally at 37.5 mg/kg twice every day. Anti-PD-L1 antibody was administered intraperitoneally every 3 d at 10 mg/kg. Tumor volume was calculated using the following formula: Tumor Volume (mm^3) = 1/2 × Length × Width.[2] Animals were sacrificed due to progressive disease if the tumor burden was greater than 2000 mm^3 or if tumor growth would surpass 2000 mm^3 before the next scheduled measurement. Bioluminescence in the LLC-luc mouse model was detected by IVIS 200 Xenogen system (IVIS

Spectrum; Perkin Elmer, Waltham, USA) after the mice were anesthetized and injected with D-luciferin.

In the tumor-fibrosis animal model, mice were anesthetized by pentobarbital sodium and received intratracheal injection of bleomycin at 2 mg/kg. Tumor cells were injected subcutaneously on 7 d later. Thorax computed tomography (CT) was scanned by using a micro-CT scanner (SkyScan 1176, Bruker, Billerica, MA, USA) and lung density was expressed as Hounsfield units (HU) used in clinical CT scanners.

Lentiviral construction and transfection

Scrambled or *Tgfb1*-specific short hairpin RNA was purchased from GeneChem (GV493, China), and used in the transduction of LLC or MC38 cells following the manufacturer's instructions. Cells were then selected in media containing 2 mg/mL puromycin (GeneChem, China). Efficiency of transfection was evaluated using western blotting and real-time RT-PCR. The sequences of mus musculus *Tgfb1* and scrambled shRNAs are as follows: shRNA 1: CGGCAGCTGTACATTGACTTT; shRNA 2: GCTCTTGTGACAGCAAAGATA; shRNA 3: AACAACGCCATCTATGAGAAA; scrambled shRNA: TTCTCCGAACGTGTCACGT.

Tumor cells isolation and flow cytometry

Tumor sections were weighed, cut into small pieces, and digested with an enzyme cocktail solution from the Mouse Tumor Dissociation Kit (Cat#130-096-730, Miltenyi Biotec) at 37°C for 30 min. The reaction was stopped by adding PBS containing 1% fetal bovine serum. Cells were pelleted at 1200rpm, 4°C for 5 min, resuspended in phosphate buffered saline, and mashed through a 70-µm cell strainer. For tumor-infiltrating lymphocyte detection, cells were separated by gradient density centrifugation using Percoll (Cat#17089109, GE life). Cells were counted using a Countstar Automated Cell Analyzer (ALIT Life Science Co., Ltd, Shanghai, China).

For flow cytometry, cells were stained according to the protocols for flow cytometry with antibodies listed in Supplementary Table S1. Data were acquired with a CytoFLEX S (Beckman Coulter) or BD LSRII cytometer and analyzed with FlowJo software (version 7.6; Tree Star, Ashland, OR, USA). Quantitation of cell populations was performed by gating from single stained positive controls and fluorescence-minus-one (FMO) controls.

CD45+ cells were isolated via magnetic-activated cell sorting (MACS) separation using Miltenyi CD45+ Microbeads (Cat#130-110-618, Miltenyi Biotec).

Western blot analysis

Western blot analysis was performed as previously described[8] using the following antibodies: anti-Smad2/3 (1:1000; CAT#8828S, Cell Signaling Technology), anti-*p*-Smad2/3 (1:1000; CAT#8685S, Cell Signaling Technology), anti-PD-L1 (1:1000, CAT#66248-1-lg, Proteintech), GAPDH (1:5000; CAT#AS1039, Aspen Biological). Briefly, tissues were homogenized, mixed with 5 X loading buffer and boiled to denaturation. The protein was separated by sodium dodecyl sulfate-

polyacrylamide gel electrophoresis and transferred to polyvinylidene fluoride membrane. Membrane was blocked with 5% nonfat milk and incubated with primary antibodies at 4°C overnight. Then, it was washed and incubated with secondary antibodies for 1 h at room temperature and visualized using SuperSignale West Pico plus Chemiluminescent Substrate (Thermo Fisher Scientifice, Waltham, MA).

RNA sequencing (RNA-seq)

For transcriptome sequencing, total RNA was isolated from the tumor tissues or CD45+ cell pellets using TRIzol reagent (Life Technologies, Carlsbad, CA, USA) and the libraries were prepared and sequenced at BGISEQ500 platform (BGI, China). Significant differential expression was set when a gene presented >1.5-fold expression difference versus the control with adjusted *p*-value of <0.05. Transcriptome data sets are available at the NCBI Sequence Read Archive with accession number PRJNA559788.

Quantitative polymerase chain reaction (qPCR)

Quantitative real-time PCR was performed as previously described[19] using gene-specific primers listed in Supplementary Table S2. Briefly, total RNA was extracted using Trizol (NO.9766, Takara Bio, Japan) and reverse transcription was performed using the PrimeScript 1st Strand cDNA Synthesis Kit (NO.6110A, Takara Bio, Japan). A Real-Time PCR System (7900HT, Applied Biosystems, USA) was utilized to run real-time PCR. Values for individual genes were standardized using GAPDH.

Micro-CT scan

Mice were anesthetized or sacrificed for thorax CT with a micro-CT scanner (Skyscan 1176, Bruker Inc, Billerica, MA). Lung slice image analysis was performed in the most typical slice that exhibited pulmonary fibrosis features. Lung density was expressed as Hounsfield units (HU) used in clinical CT scanners.

Lung histology and fibrosis score

Lung histological analysis was conducted as previously described.[8] Briefly, lung tissue was fixed in 4% formalin and embedded in paraffin, and subsequently cut into 5-μm thick sections and stained with hematoxylin and eosin (H&E) and Masson's trichrome (Aspen Biological, Wuhan, China). The sections stained with Masson's trichrome were subjected to Ashcroft score by two senior pathologists blinded to the experimental information.

Immunohistochemistry (IHC)

Tissue sections were deparaffinized, rehydrated, blocked of endogenous peroxidase and subjected to antigen retrieval, and then immediately incubated with 5% bovine serum albumin at room temperature for 1 h, followed by incubation with the anti-CD3 antibodies (1:200, CAT#ab16669, Abcam) at 4°C overnight. The slides were then reacted with peroxidase polymer-conjugated secondary antibody (1:5,000) and DAB (both from Aspen Biological) followed by counterstaining with hematoxylin.

For CD3+T cell counting, five fields (200X) in the tumor periphery or tumor center were randomly selected and imaged using a light microscope (Olympus Corporation, Tokyo, Japan). Positive cells were manually counted by the blinded pathologists.

In *vivo* biosafety evaluation

For blood biochemistry evaluation, serum was collected as described above and analyzed in Wuhan Servicebio Technology CO., Ltd. by a Chemray 240 Automatic Biochemical Analyzer (Rayto Science, Shenzhen, China). To evaluate histopathological damage, major organs (heart, liver, lung, colon, and kidney) were excised, fixed in 4% paraformaldehyde, embedded in paraffin, and cut into 6-μm sections for hematoxylin and eosin (H&E) staining by standard procedures. Images were captured using a light microscope (Olympus Corporation).

Statistical analysis

Statistical analysis was performed using GraphPad Prism (GraphPad Software, San Diego, CA, USA) or SPSS software (SPSS Inc., Chicago, IL, USA). The unpaired Student's t-test was used to compare differences between two groups, while one-way ANOVA was used to compare differences between multiple groups. For animal experiments, we used repeated-measures ANOVA with Tukey's multiple comparison test. Mouse survival curves were calculated using the Kaplan–Meier method and compared by the log-rank test. Data were expressed as the mean ± standard error of mean (SEM) or ± standard deviation (SD) as stated in the figure legends. $P < .05$ was considered significant.

Results

Pirfenidone monotherapy induced tumor regression only in immunocompetent mice

To investigate the role of PFD in antitumor immunity, we compared the antitumor effects of PFD between immunocompetent (C57BL/6) and immunocompromised (athymic nude) mice. Mice were inoculated with 1×10^6 LLC-luc cells. When tumors reached ~100 mm^3 (day 0), PFD was administered orally at 500 mg/kg once every day (Figure 1(a)). We observed a reduced tumor burden in immunocompetent mice in PFD treated group by calculating tumor volumes (Figure 1(b), $p = .038$) as well as bioluminescence imaging (Figure 1(d), $p = .0304$). However, this tumor-control effect was not observed in immunodeficient mice (Figure 1(c, e)). PFD also failed to reduce the lesion development in immunodeficient mice inoculated with the human lung cancer cell lines A549 and H292 (Fig. S1). These results suggested that the antitumor effect of PFD requires an intact immune system.

Pirfenidone suppressed the TGFβ signaling pathway and activated the antitumor immune response

LLC-luc tumors from pirfenidone-treated or vehicle control-treated mice were harvested 9 d after therapy initiation and the changes in immune cell infiltration were analyzed by flow
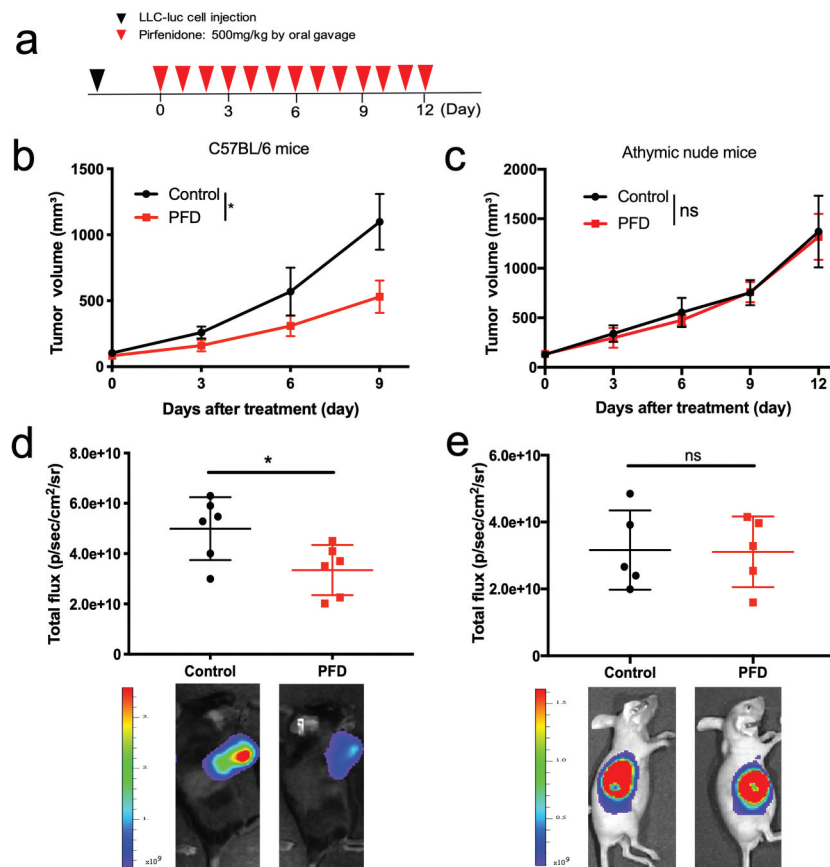
Figure 1. PFD monotherapy induces tumor regression only in immunocompetent mice. C57BL/6 mice (n = 6 per group) or Balb/c nude mice (n = 5 per group) were subcutaneously engrafted with LLC-luc cells, after tumor establishment, treated orally with PFD. (a) Diagram of the experimental protocol. (b, c) Tumor volume measured over time. Data were analyzed using repeated-measures ANOVA and represented as means ± SEM. (d, e) Top: quantification of bioluminescent imaging on day 9, data were analyzed using Student's *t*-test; Bottom: endpoint images. *, *p*< .05; ns, not significant.

cytometry. Although the density (cell number per gram of tumor weight) of total immune cells (CD45+) was not changed by PFD treatment (Fig. S2a), there was an increase in the density of CD8+ cytotoxic T cells (Figure 2(a), p = .0368). Moreover, there was a decrease in the density of myeloid-derived suppressor cells (MDSCs) (Figure 2(b), p = .0417), which are known to promote immunosuppression in the tumor microenvironment. Du *et al.* reported that pirfenidone can ameliorate murine chronic graft-versus-host disease through inhibition of macrophage infiltration.[20] However, in the present study, the density of tumor-associated macrophages and the ratio of M2 to M1 macrophages (M2/M1) remained unchanged by PFD (Fig. S2b).

TGF-β is initially complexed with latency-associated peptide (LAP), and LAP expression correlates with TGF-β production in many cell types.[21,22] As shown in Figure 2(c), PFD treatment significantly decreased the membrane expression of LAP in total live cells (p = .039). Moreover, we noted a decreased phosphorylation of Smad2/3 in the tumor homogenates (Figure 2(d)). To verify whether PFD acts through the TGFβ signaling pathway, stably *Tgfb1* knockdown (KD) MC38 cells were generated and inoculated onto C57BL/6 mice (Fig. S2c). As shown in Figure 2(e), while PFD significantly reduced the growth of scrambled control tumors (Scrambled control vs. Scrambled PFD, P < .001), it failed to control the proliferation of *Tgfb1* KD tumors (*Tgfb1*-KD vs. *Tgfb1*-KD+PFD, P = .164).

These results suggest that the antitumor efficacy of PFD is achieved, at least partially, by suppressing TGFβ signaling pathway.

CD45+ cells were separated from the control and PFD treated tumors and RNA-seq was performed. Gene set enrichment analysis (GSEA) showed that PFD treatment elevated the expression of immune-associated genes, which were significantly enriched in "positive regulation of interferon gama production" (Figure 2(f)) and "positive regulation of T cell proliferation" (Figure 2(g)). Other pathways such as "immune response", "adaptive immune response" and "T cell receptor signaling pathway" were also significantly enriched (Table S3). These results suggested that PFD treatment activated the antitumor immune response.

Combining pirfenidone with PD-L1 blockade induced synergic antitumor effects in mouse models

Three syngeneic tumor models that differ in their sensitivity to PD-L1 blockade were used to investigate whether PFD could synergize with PD-L1 checkpoint blockade. Mice were treated as indicated in Figure 3(a).

In the poorly immunogenic LLC-luc mouse models, treatment with anti-PD-L1 alone did not reduce tumor burden at any time point after treatment; PFD alone modestly reduced
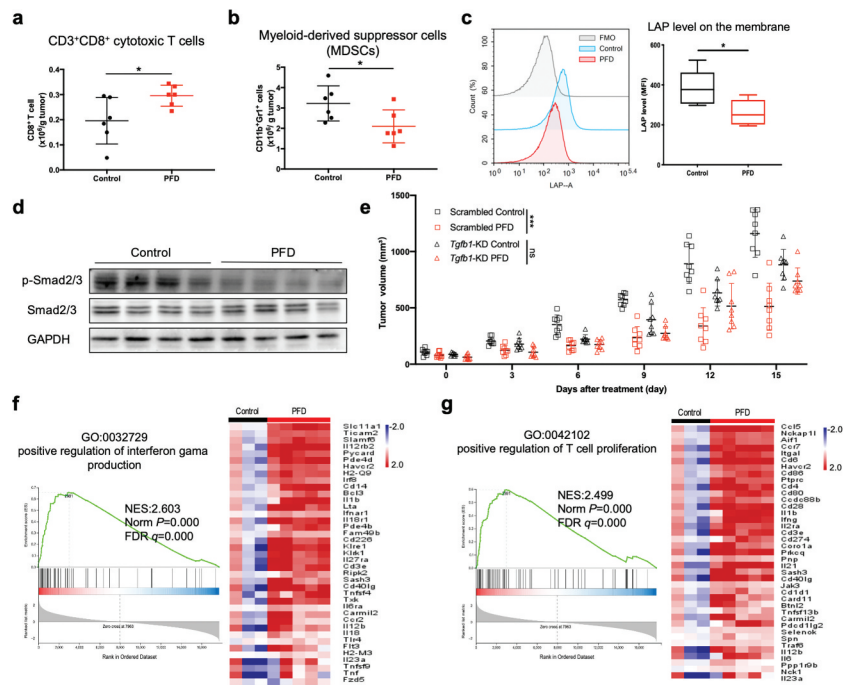
Figure 2. Pirfenidone suppressed the TGFβ signaling pathway and activated the anti-tumor immune response. (a) The absolute number of cytotoxic T cells in LLC-luc tumors on day 9. (b) The absolute number of myeloid-derived suppressor cells (MDSCs) on day 9. (c) Mean fluorescence intensities (MFI) of LAP in the membranes of total live cells in the tumors. FMO: fluorescence-minus-one control. (d) Expression of *p*-Smad2/3 in total tumor homogenate. (e) C57BL/6 mice were subcutaneously inoculated with MC38 scrambled or *Tgfb1*-KD cells and treated orally with PFD. Tumor volume was measured over time. (f and g) Left: GSEA plots for RNA-seq data of CD45+ cells isolated from control (n = 3) or PFD treated (n = 5) tumors. Normalized enrichment score (NES) and FDR *q* value are stated on the plots. Right: genes in the two representative gene sets are labeled in respective heatmaps. Statistical significance in (**a ~ c**) was measured by Student's *t*-test and represented as means ± SD, that in (**e**) was analyzed using repeated-measures ANOVA with Tukey's test. *, *p* < .05; **, *p* < .01; ***, *p* < .001; ns, not significant.

the tumor burden in the early phase but failed to control tumor progression in later periods. Combination therapy significantly delayed tumor growth when compared with control or anti-PD-L1 alone (Figure 3(b)). Although the difference in tumor growth suppression at early time points was not significantly different between the combination therapy and PFD mono-therapy, the long-term survival of mice was significantly better in the combination group (PFD vs. PFD+anti-PD-L1, *p* = .042, log-rank test) (Figure 3(c)). The individual tumor growth curves are shown in Fig. S3a.

MC38 murine colorectal adenocarcinoma is responsive to ICIs in some studies;[23,24] however, it is poorly immunogenic in others.[16,25,26] As is shown in the individual tumor growth curves (Fig. S3b), while few mice in the anti-PD-L1 monother-apy groups responded to the treatment, 5 of 10 mice showed delayed tumor growth in the combination group. Among these five mice, three mice sustained standard disease during the 21-day treatment and maintained it for another 2 weeks before tumors developed. Compared to the control and monotherapy groups, treatment with PFD plus anti–PD-1 antibodies aug-mented the anti-tumor response, reflected in significantly reduced tumor size (Figure 3(d)). Combination therapy also significantly prolonged the survival of mice beyond that observed for the control and monotherapy groups (Figure 3(e)).

Preliminary, unpublished studies in our laboratory suggest that H22 murine hepatocellular carcinoma is an immune-responsive tumor model which is regressed with four doses of anti-PD-L1 antibody. In this tumor model, although anti-PD-L1 had statistically significant antitumor activity (*P* = .002),

combination therapy inhibited tumor growth more strongly than anti-PD-L1 alone (*P* = .048) (Figure 3(f)). Combination therapy also showed great survival benefit in this tumor model (Figure 3(g)). Over a 55-day observation period, complete tumor regression was observed in four mice (40%) treated with combination regimen, compared with only two mice treated with PD-L1 blockades alone (20%) (Fig. S3c).

Combination therapy produces inflammatory immune gene-expression signatures

An unbiased RNA sequencing (RNA-seq) was performed to quantify changes in gene expression induced by PFD and/or anti-PD-L1 treatment. Relative to untreated controls, PFD, anti-PD-L1, and combination treatments resulted in the differ-ential expression (defined as *P* < .05 and a fold change >1.5) of 1403, 1338, and 1438, respectively, of 30315 total genes eval-uated (Figure 4(a)). The functional classification of the differ-entially expressed genes (DEGs) was carried out based on the Gene Ontology (GO). The top 10 most significantly enriched GO terms (biological process) in each group are listed in Figure 4(b). Interestingly, all three treatments significantly altered genes implicated in the "immune response", demonstrating that both monotherapy and combination therapy modulated genes related to the immune response. A considerable number of DEGs in the combination treatment were also enriched in the categories of "inflammatory response", "innate immune response", and "positive regulation of B-cell activation", sug-gesting that combination therapy markedly altered gene
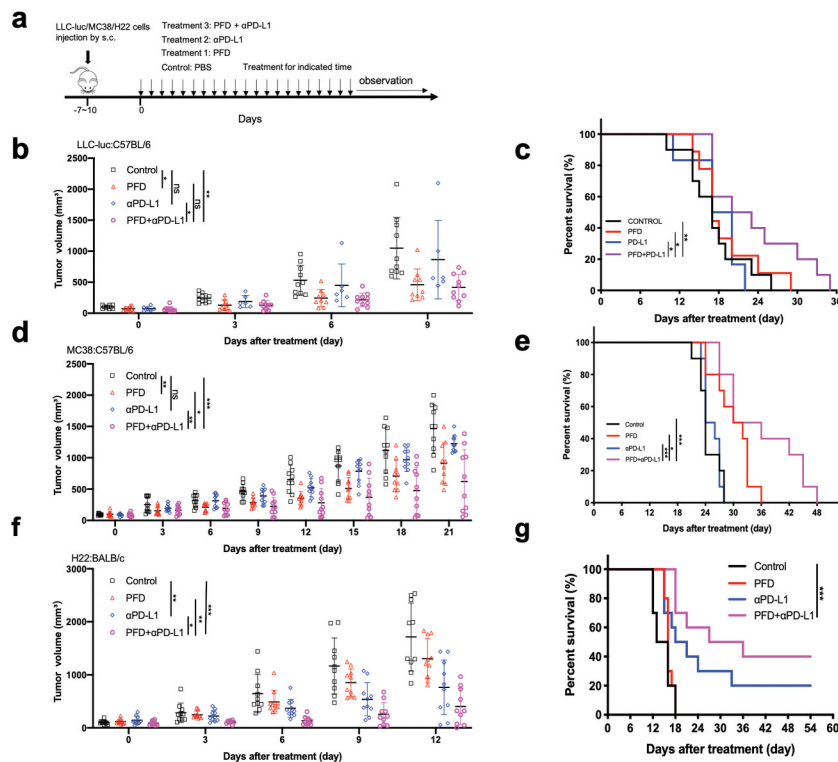
Figure 3. Combining PFD with anti-PD-L1 antibody delays tumor growth and prolongs the survival of tumor-bearing mice. For LLC-luc or MC38 tumors, anti-PD-L1 antibody was administered every 3 d for a total of 7 doses; for H22 tumor, a total of 4 doses of anti-PD-L1 antibody were administered. (a) Diagram of the experimental protocol. (b) LLC-luc tumor volumes were assessed at indicated time points. (n = 6 ~ 10 per group). (c) Survival of mice bearing LLC-luc tumors following treatment. (d) MC38 tumor volumes were assessed at indicated time points. (n = 10 per group). (e) Survival of mice bearing MC38 tumors following treatment. (f) H22 tumor volumes were assessed at indicated time points. (n = 10 per group). (g) Survival of mice bearing H22 tumors following treatment. These experiments were repeated once with similar results. Statistical significance in **(b, d and f)** was measured by repeated-measures ANOVA with Tukey's test, that in **(c, e and g)** was analyzed using the Kaplan-Meier method and compared by the log-rank test. *, $p < .05$; **, $p < .01$; ***, $p < .001$; ns, not significant.

expression related to the inflammation and the immune system.

Notably, more than half of the DEGs in the combination group were unique compared to those in the monotherapy groups (Figure 4(c) and Table S4), demonstrating that combination therapy induced a unique signature compared with monotherapy. As depicted in the volcano plot (Figure 4(d)), combination treatment induced an inflamed immune signature, exemplified by an upregulation of genes including *Ccl3, Ccl4, Ccl5* (known to recruit monocytes and macrophages), *Cxcl1, Cxcl2, Cxcl3, Cxcl5, Cxcl12* (known to recruit TH17, DC, and B cells), *Cxcl13, Gzma, Tnf, and Ifng* (T cell activation-associated genes) .[27] We performed quantitative RT-PCR using gene-specific primers to confirm the expression patterns of these genes and found that they were consistent with observations from RNA-seq (Figure 4(e)). Together, these findings demonstrated that combination therapy induced a unique signature compared with monotherapy, which was characterized by an increased expression of cytokines and chemokines.

Combination treatment increased infiltration of T cells in the tumor microenvironment

We further investigated whether combination treatment increased infiltration of T cells into the center of tumor by IHC and flow cytometry. As detected by IHC, CD3⁺ T cell distribution was significantly changed following combination therapy, with more CD3⁺ T cells gathering in the center of tumor rather than being restricted to the tumor stromal (Figure 5(a, b)). We also observed a significantly increased infiltration of CD45⁺ immune cells (Figure 5(c)) and a decreased infiltration of MDSC (Figure 5(d)) in the combination group as detected by flow cytometry. Similarly, there was an increase in the density of CD3⁺ T cells (Figure 5(e)) as well as CD8⁺ T cells (Figure 5(f)) in the combination treatment group.

Combination treatment showed promising effect in alleviating pulmonary fibrosis and controlling tumor growth in the tumor-fibrosis model

The tumor-fibrosis model was created by intratracheally administrating of bleomycin and subcutaneously injecting tumor cells 7 d later. Combination treatment was administered when the tumor was well established (Figure 6(a)). In this model, we also conducted a side-by-side comparison between PFD vs. galunisertib, an orally active small molecule inhibitor of TGFβ receptor I (TGFβRI) which already showed an anti-tumor effect in pre-clinical tumor models at a dose of 37.5 mg/kg BID.[17]

As shown in the CT scan (Figure 6(b)), while obvious pulmonary consolidation and elevated lung density were observed in the entire lung in the control mice, the radiological signs of fibrosis were significantly reduced in the PFD+ICI group. The benefit of
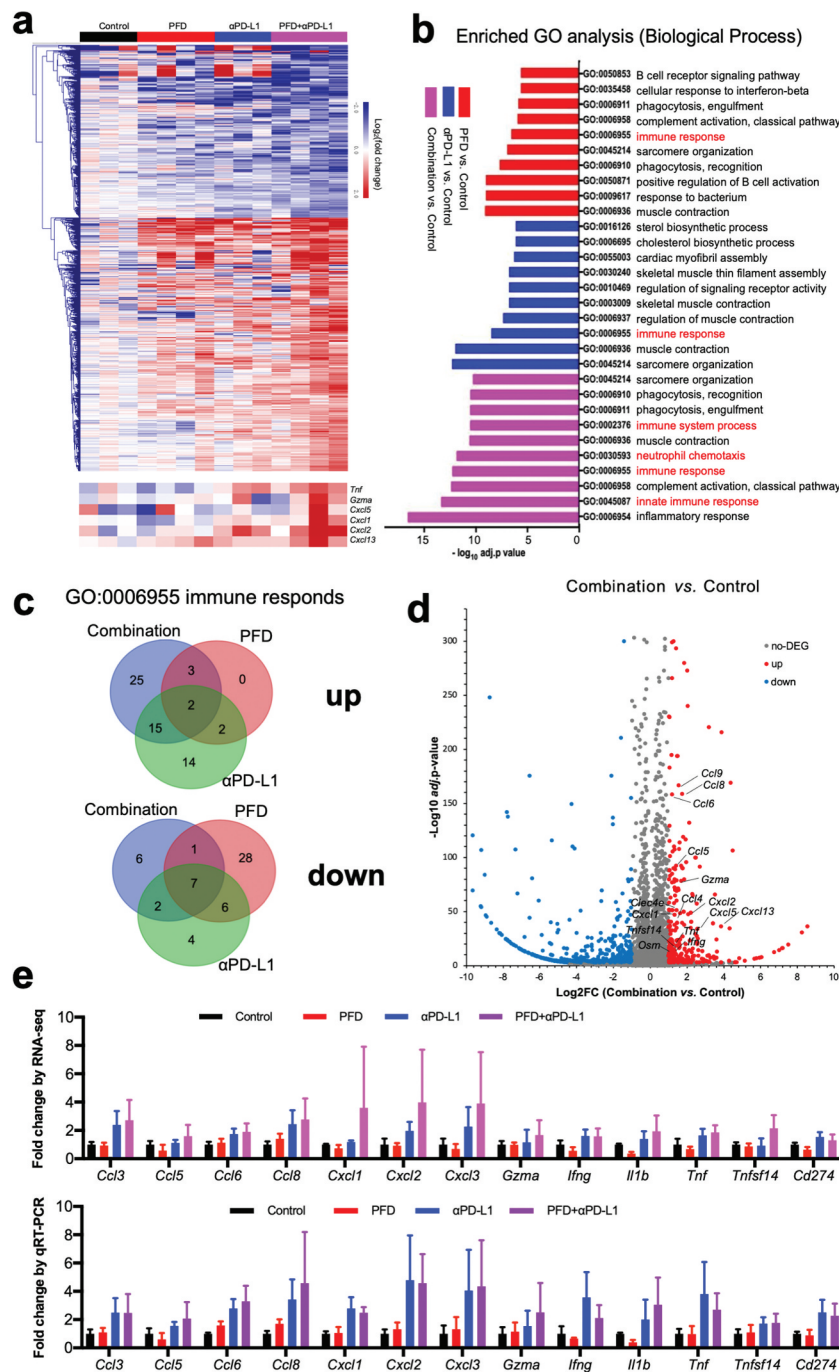
Figure 4. Combining PFD with anti-PD-L1 produces a markedly inflamed immune gene signature. Mice bearing MC38 tumors were treated for 9 d and tumors were analyzed by RNA sequencing (RNA-seq). (a) Heat map of gene expression changes for all significantly differentially expressed genes (defined as $P < .05$ and a fold change of > 1.5) from RNA-seq analysis. Colors in each box represent the log2(fold change) in the expression of each gene after treatment relative to the median control; rows represent individual genes, and columns represent individual mice. (n = 3 in control and anti-PD-L1 groups, n = 4 in PFD and combination groups). The magnified heat map in the below shows the expression of *Tnf, Gzma, Cxcl5, Cxcl1, Cxcl2, and Cxcl12*. (b) The 10 most significantly enriched GO terms across experimental groups. (c) Venn diagrams showing the number of shared and treatment-specific DEGs in each group for the GO term "immune response". (d) Volcano plot of selected DEGs in the combination group relative to control. (e) qRT-PCR validation of selected genes identified by RNA-seq. (n = 5 per group).

treatment was further confirmed by pathological method as H□E and Masson's trichrome staining revealed a significantly alleviated pulmonary fibrosis in PFD+ICI group (Figure 6(c)). Galunisertib plus ICI treatment led to a small but non-significant reduction in lung density and fibrosis score (Figure 6(c, d)). Furthermore, we observed a stronger tumor regression in PFD+ICI group when compared to the tumor growth curve with galunisertib+ICI group (Figure 6(c)), $P = .036$). In conclusion, PFD showed a significant advantage over galunisertib in alleviating pulmonary fibrosis and promoting the antitumor immunity.

Combination therapy is safe *in vivo*

The results summarized above demonstrate that combining PFD with PD-L1 blockade delayed the tumor growth alleviated
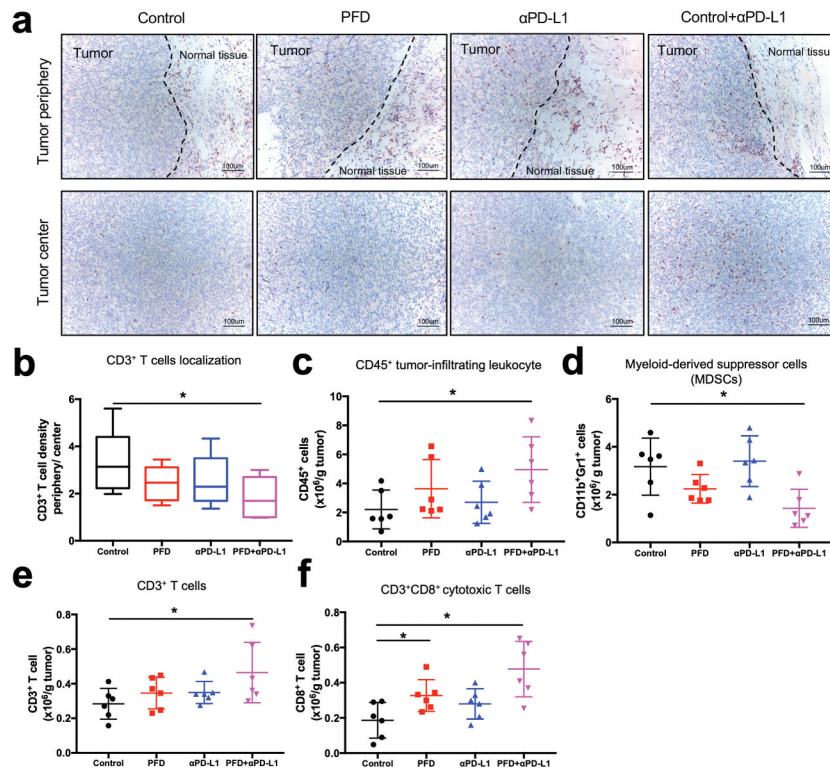
Figure 5. Combination treatment increases infiltration of T cells into the tumor microenvironment. MC38 tumors (n = 6 per group) were harvested on day 9 and IHC and flow cytometry analyses were performed. (a) Representative CD3 staining (200X) of tumor periphery (top) and center (below). Scale bar, 100 µm. (b)Number of CD3+ T cells in the periphery as well as in the center were counted and the ratio of CD3+ T cells in the periphery relative to the center was calculated. (c-f) Flow cytometry analysis was performed and absolute numbers of CD45+ cells (c), MDSC cells (d), CD3+ T cells (e) and CD3+CD8+ cytotoxic T cells (f) per 1.0 g of tumor tissue were calculated. Experiments were repeated twice with similar results. Data was analyzed by one-way ANOVA with Dunnett's multiple comparison *, $p < .05$; ns, no significant.
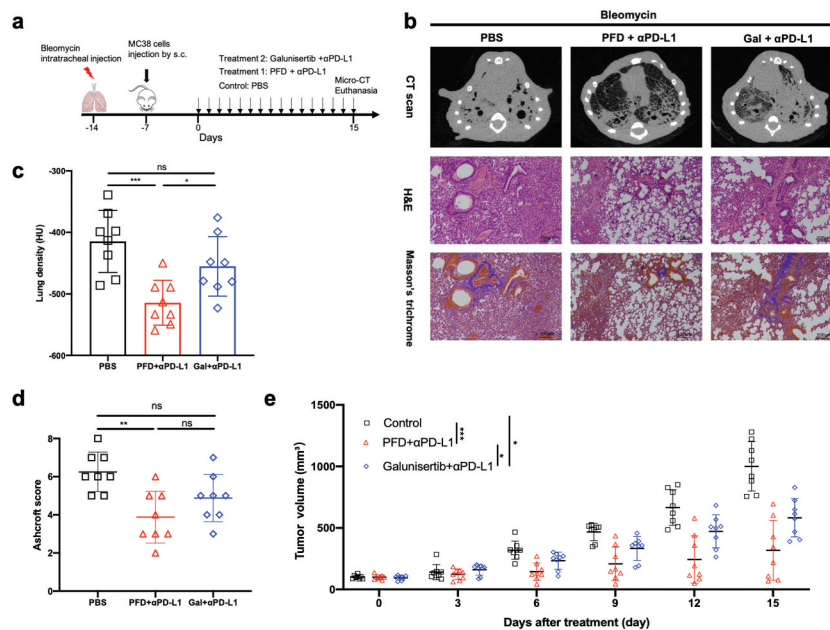

Figure 6. Combination treatment showed promising effect in alleviating pulmonary fibrosis and controlling tumor growth in the tumor-fibrosis model. (a) Diagram of the experimental protocol. (b) Representative images of CT scan, H&E and Masson's trichrome staining (100X) of mice from different group. (c) Hounsfield units (HU) derived from CT scans. HUs are defined on the basis of − 1,000 for air and 0 for water. (d) Fibrosis scores for grading lung histopathological changes. (e) MC38 tumor volumes were assessed at indicated time points. (n = 8 per group). Statistical significance in (c, d) was measured by one-way ANOVA with Dunnett's multiple comparison, that in **(e)** was measured by repeated-measures ANOVA with Tukey's test *, $p < .05$; **, $p < .01$; ***, $p < .001$; ns, not significant.

the pulmonary fibrosis. However, in clinical practice, biosafety of the combination regimen is a primary concern. Therefore, we performed a toxicological evaluation to study whether combination treatment had a safe toxicological profile. We

monitored body weight as a general indicator of health status. No significant differences were observed over 9 d of treatment (Figure 7(a)). Subsequently, mice were euthanized for blood biochemistry and histological analyses. Serum alanine aminotransferase (ALT, Figure 7(b)), aspartate aminotransferase (AST, Figure 7(c)), blood urea nitrogen (BUN, Figure 7(d)), creatinine (CRE, Figure 7(e)), and lactate dehydrogenase (LDH-L, Figure 7(f)) were measured to evaluate the liver, renal, and heart damages. Their levels were found to be within the normal range. The major organs (heart, liver, lung, kidney, and colon) were subjected to H&E staining (Figure 7(g)). No signs of dysfunctional pathology such as inflammation, injury, and necrosis were observed in the treatment group. These results indicated that there were no obvious signs of autoimmunity or drug toxicity in mice treated with the combination regimen.

Discussion

In clinic trails as well as real-world experience, PFD is a well-tolerated oral medication that shows encouraging results in reducing the decline of respiratory function in IPF patients.[28,29] In a retrospective study, a reduced incidence of lung cancer under PFD therapy has been observed in IPF patients.[30] In addition, perioperative PFD treatment reduced postoperative acute exacerbation in lung cancer patients with comorbid IPF.[31] These evidences showed PFD may have preventive or treatment function for lung cancer beside its antifibrotic property. Indeed, multiple in vitro studies reported decreased proliferation and migration of cancer cells following exposure to PFD.[32–36] However, in immunocompromised mice inoculated with tumor xenograft, the antitumor effect of single-agent PFD is largely limited. For example, PFD alone did not affect tumor growth of SUIT-2 cell (pancreatic cancer cells) xenografts; it suppressed tumor growth only when SUIT-2 cells were co-implanted with pancreatic stellate cells.[33] Furthermore, PFD alone did not reduce tumor proliferation of mesothelioma xenografts[37] and NSCLC xenografts.[38] These studies together suggested that PFD exerted its ability mainly through inhibiting desmoplasia, suppressing tumor–stromal interactions and increasing chemotherapeutic drugs infiltration in the tumor. However, early studies using immunocompromised animals may be incomprehensive as the immune modulation effect of PFD will be neglected.

In the present study, we show that PFD monotherapy induces tumor regression only in immunocompetent mice. It increases the infiltration of CD8+ cytotoxic T cells and decreased the infiltration of MDSCs. Furthermore, it shows synergistic effect with PD-L1 blockade in three syngeneic tumor models. RNA-seq reveals that combination therapy induced an inflamed immune signature, which was characterized by an increased expression of cytokines and chemokines.
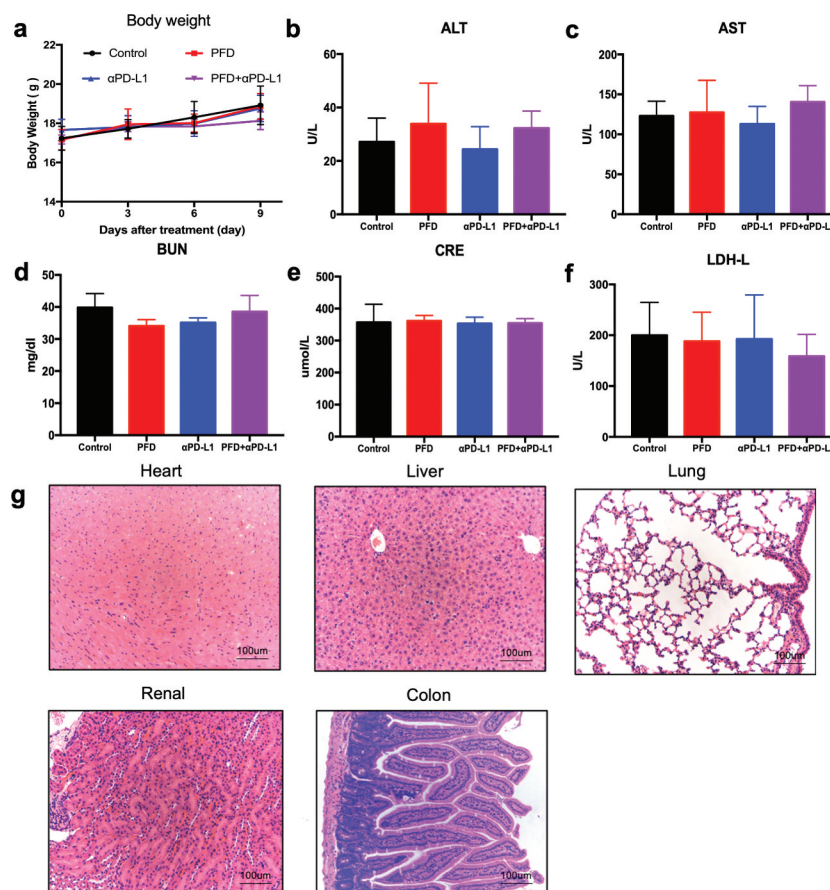

Figure 7. Combination treatment is biologically safe in vivo. Tumor-bearing mice were treated for 9 d and sacrificed for blood and organ collection. (a) Body weight of mice was measured. (b-f) Serum alanine aminotransferase (ALT), aspartate aminotransferase (AST), blood urea nitrogen (BUN), creatinine (CRE), and lactate dehydrogenase (LDH-L) were measured (n = 6 for each group, the experiment was repeated twice.). (g) Representative image of H&E staining (200X) of the heart, liver, lung, kidney, and colon of mice in the combination group.

Based on our studies and the published literature, we believe that PFD reduces the tumor growth not by directly controlling cancer cell proliferation, but through regulating the extracellular matrix and the immune compartment. In *TGFβ1* knock down tumors, the antitumor effect of PFD was abolished. Therefore, PFD exerts its antitumor ability, at least partially, by suppressing TGFβ signaling pathway.

TGFβ is a pleiotropic cytokine which plays an important role in tissue fibrosis, cancer development and immune evasion. Several pharmacological approaches to block TGFβ signaling, including neutralizing antibodies, vaccines, antisense oligonucleotides and small molecular inhibitors, have shown promising results in preclinical studies.[39] However, long-term continuous exposure to TGF-β inhibitors may lead to undesirable side effects such as heart valve lesions and aortic aneurysms, which restrict their clinical application.[39] Galunisertib is an orally active small molecule inhibitor of the TGFβRI which showed promising antifibrosis[40] and antitumor activities[17,41] in preclinical models. In our study using tumor-fibrosis model, however, PFD showed better effect than galunisertib in alleviating pulmonary fibrosis and controlling tumor growth.

In clinical practice, PFD is prescribed to IPF patients at 801 mg three times daily (2403 mg per day).[1] In the present study, a dose of 500 mg/kg/day was administered to animals, which corresponded to 2432 mg/day when converted to 60-kg human usage based on body surface area.[42] Since this is a litter higher than the dosage prescribed for humans, our data suggest that administering PFD concomitantly with anti-PD-L1 antibody would have no negative toxicological effects on the liver or renal function.

There are some limitations to our study. Firstly, we failed to observe a robust effect of the combination treatment as we anticipated, especially in the poorly immunogenic mouse models. Thus, further exploration of PFD as part of PD-1/L1-based combination therapy with radiotherapy or chemotherapy should be considered. Secondly, we did not devise an ideal approach to dynamically measure the leukocyte infiltration. Whether the alteration in the extracellular fibers played a role in enhancing the leukocyte infiltration remains unknown. Thirdly, the exact molecular mode of action of PFD on immune activation is still a question needed to be further explored.

In conclusion, our study identified a novel function of PFD that it could enhance the antitumor effect of PD-L1 blockade by increasing the expression of cytokines and chemokines, and promoted T cell infiltration. Our initial findings encourage the further clinical trials to determine the efficacy of the combination of PFD with PD-L1 inhibitors, particularly, in lung cancer patients with comorbid IPF.

Declaration of interest statement

The authors declare no conflict of interest.

Disclosure statement

The authors report no conflict of interest.

References

1. Lederer DJ. Martinez FJ: idiopathic pulmonary fibrosis. N Engl J Med. 2018;378:1811–1823. doi:10.1056/NEJMra1705751.
2. Zielinski M, Sitek P. Ziora D: idiopathic pulmonary fibrosis coexisting with lung cancer - a review. Adv Respir Med. 2018;86 (6):319–326. doi: 10.5603/ARM.a2018.0052.
3. Tzouvelekis A, Gomatou G, Bouros E, Trigidou R, Tzilas V, Bouros D. Common pathogenic mechanisms between idiopathic pulmonary fibrosis and lung cancer. Chest. 2019. doi:10.1016/j.chest.2019.04.114.
4. Sato T, Watanabe A, Kondo H, Kanzaiki M, Okubo K, Yokoi K, Marutsuka T, Shinohara H, Teramukai S, Kishi K, et al. Long-term results and predictors of survival after surgical resection of patients with lung cancer and interstitial lung diseases. J Thorac Cardiovasc Surg. 2015;149(64–69):70 e61–62. doi:10.1016/j.jtcvs.2014.08.086.
5. Chen H, Senan S, Nossent EJ, Boldt RG, Warner A, Palma DA, Louie AV. Treatment-related toxicity in patients with early-stage non-small cell lung cancer and coexisting interstitial lung disease: a systematic review. Int J Radiat Oncol Biol Phys. 2017;98 (3):622–631. doi:10.1016/j.ijrobp.2017.03.010.
6. Kudoh S, Kato H, Nishiwaki Y, Fukuoka M, Nakata K, Ichinose Y, Tsuboi M, Yokota S, Nakagawa K, Suga M, et al. Interstitial lung disease in Japanese patients with lung cancer: a cohort and nested case-control study. Am J Respir Crit Care Med. 2008;177 (12):1348–1357. doi:10.1164/rccm.200710-1501OC.
7. Raghu G, Rochwerg B, Zhang Y, Garcia CAC, Azuma A, Behr J, Brozek JL, Collard HR, Cunningham W, Homma S, et al. An official ATS/ERS/JRS/ALAT clinical practice guideline: treatment of idiopathic pulmonary fibrosis. An update of the 2011 clinical practice guideline. Am J Respir Crit Care Med. 2015;192(2):e3–19. doi:10.1164/rccm.201506-1063ST.
8. Qin W, Liu B, Yi M, Li L, Tang Y, Wu B, Yuan X. Antifibrotic agent pirfenidone protects against development of radiation-induced pulmonary fibrosis in a murine model. Radiat Res. 2018;190 (4):396–403. doi:10.1667/RR15017.1.
9. Selvaggio AS. Noble PW: pirfenidone initiates a new era in the treatment of idiopathic pulmonary fibrosis. Annu Rev Med. 2016;67:487–495. doi:10.1146/annurev-med-120214-013614.
10. Kwapiszewska G, Gungl A, Wilhelm J, Marsh LM, Thekkekara Puthenparampil H, Sinn K, Didiasova M, Klepetko W, Kosanovic D, Schermuly RT, et al. Transcriptome profiling reveals the complexity of pirfenidone effects in IPF. Eur Respir J. 2018;1800564. doi:10.1183/13993003.00564-2018
11. Aboulkheyr Es H, Zhand S, Thiery JP, Warkiani ME. Pirfenidone reduces immune-suppressive capacity of cancer-associated fibroblasts through targeting CCL17 and TNF-beta. Integr Biol (Camb). 2020;12(7):188–197. doi:10.1093/intbio/zyaa014.
12. Marwitz S, Turkowski K, Nitschkowski D, Weigert A, Brandenburg J, Reiling N, Thomas M, Reck M, Dromann D, Seeger W, et al. The multi-modal effect of the anti-fibrotic drug pirfenidone on NSCLC. Front Oncol. 2019;9:1550. doi: 10.3389/fonc.2019.01550.
13. Gubens MA. Davies M: NCCN guidelines updates: new immunotherapy strategies for improving outcomes in non-small cell lung cancer. J Natl Compr Canc Netw. 2019;17:574–578.

14. Gajewski TF. The next hurdle in cancer immunotherapy: overcoming the non-T-cell-inflamed tumor microenvironment. Semin Oncol. 2015;42:663–671. doi:10.1053/j.seminoncol.2015.05.011.

15. Tauriello DVF, Palomo-Ponce S, Stork D, Berenguer-Llergo A, Badia-Ramentol J, Iglesias M, Sevillano M, Ibiza S, Cañellas A, Hernando-Momblona X, et al. TGFbeta drives immune evasion in genetically reconstituted colon cancer metastasis. Nature. 2018;554:538–543. doi:10.1038/nature25492.

16. Mariathasan S, Turley SJ, Nickles D, Castiglioni A, Yuen K, Wang Y, Kadel III EE, Koeppen H, Astarita JL, Cubas R, et al. TGFbeta attenuates tumour response to PD-L1 blockade by contributing to exclusion of T cells. Nature. 2018;554(7693):544–548. doi:10.1038/nature25501.

17. Holmgaard RB, Schaer DA, Li Y, Castaneda SP, Murphy MY, Xu X, Inigo I, Dobkin J, Manro JR, Iversen PW, et al. Targeting the TGFβ pathway with galunisertib, a TGFβRI small molecule inhibitor, promotes anti-tumor immunity leading to durable, complete responses, as monotherapy and in combination with checkpoint blockade. J Immuno Ther Cancer. 2018;6(1). doi:10.1186/s40425-018-0356-4.

18. Lan Y, Zhang D, Xu C, Hance KW, Marelli B, Qi J, Yu H, Qin G, Sircar A, Hernández VM, et al. Enhanced preclinical antitumor activity of M7824, a bifunctional fusion protein simultaneously targeting PD-L1 and TGF-beta. Sci Transl Med. 2018;10. doi:10.1126/scitranslmed.aan5488

19. Yi M, Liu B, Tang Y, Li F, Qin W, Yuan Xianglin. Irradiated human umbilical vein endothelial cells undergo endothelial-mesenchymal transition via the snail/miR-199a-5p axis to promote the differentiation of fibroblasts into myofibroblasts. Biomed Res Int. 2018;4135806:2018

20. Du J, Paz K, Flynn R, Vulic A, Robinson TM, Lineburg KE, Alexander KA, Meng J, Roy S, Panoskaltsis-Mortari A, et al. Pirfenidone ameliorates murine chronic GVHD through inhibition of macrophage infiltration and TGF-beta production. Blood. 2017;129:2570–2580. doi:10.1182/blood-2017-01-758854.

21. Ochi H, Abraham M, Ishikawa H, Frenkel D, Yang K, Basso AS, Wu H, Chen M-L, Gandhi R, Miller A, et al. Oral CD3-specific antibody suppresses autoimmune encephalomyelitis by inducing CD4+ CD25- LAP+ T cells. Nat Med. 2006;12:627–635. doi:10.1038/nm1408.

22. Gandhi R, Anderson DE. Weiner HL: cutting edge: immature human dendritic cells express latency-associated peptide and inhibit T cell activation in a TGF-beta-dependent manner. J Immunol. 2007;178:4017–4021. doi:10.4049/jimmunol.178.7.4017.

23. Lin H, Wei S, Hurt EM, Green MD, Zhao L, Vatan L, Szeliga W, Herbst R, Harms PW, Fecher LA, et al. Host expression of PD-L1 determines efficacy of PD-L1 pathway blockade-mediated tumor regression. J Clin Invest. 2018;128:1708. doi:10.1172/JCI120803.

24. Juneja VR, McGuire KA, Manguso RT, LaFleur MW, Collins N, Haining WN, Freeman GJ, Sharpe AH. PD-L1 on tumor cells is sufficient for immune evasion in immunogenic tumors and inhibits CD8 T cell cytotoxicity. J Exp Med. 2017;214(4):895–904. doi:10.1084/jem.20160801.

25. Mosely SI, Prime JE, Sainson RC, Koopmann J-O, Wang DYQ, Greenawalt DM, Ahdesmaki MJ, Leyland R, Mullins S, Pacelli L, et al. Rational selection of syngeneic preclinical tumor models for immunotherapeutic drug discovery. Cancer Immunol Res. 2017;5 (1):29–41. doi:10.1158/2326-6066.CIR-16-0114.

26. D'Alterio C, Buoncervello M, Ierano C, Napolitano M, Portella L, Rea G, Barbieri A, Luciano A, Scognamiglio G, Tatangelo F, et al. Targeting CXCR4 potentiates anti-PD-1 efficacy modifying the tumor microenvironment and inhibiting neoplastic PD-1. J Exp Clin Cancer Res. 2019;38:432.

27. Nagarsheth N, Wicha MS. Zou W: chemokines in the cancer microenvironment and their relevance in cancer immunotherapy. Nat Rev Immunol. 2017;17:559–572.

28. Noble PW, Albera C, Bradford WZ, Costabel U, Glassberg MK, Kardatzke D, King TE, Lancaster L, Sahn SA, Szwarcberg J, et al. Pirfenidone in patients with idiopathic pulmonary fibrosis (CAPACITY): two randomised trials. Lancet. 2011;377 (9779):1760–1769. doi:10.1016/S0140-6736(11)60405-4.

29. King TE Jr, Bradford WZ, Castro-Bernardini S, Fagan EA, Glaspole I, Glassberg MK, Gorina E, Hopkins PM, Kardatzke D, Lancaster L, et al. A phase 3 trial of pirfenidone in patients with idiopathic pulmonary fibrosis. N Engl J Med. 2014;370:2083–2092.

30. Miura Y, Saito T, Tanaka T, Takoi H, Yatagai Y, Inomata M, Nei T, Saito Y, Gemma A, Azuma A, et al. Reduced incidence of lung cancer in patients with idiopathic pulmonary fibrosis treated with pirfenidone. Respir Investig. 2018;56(1):72–79. doi:10.1016/j.resinv.2017.09.007.

31. Kanayama M, Mori M, Matsumiya H, Taira A, Shinohara S, Kuwata T, Imanishi N, Yoneda K, Kuroda K, Tanaka F, et al. Perioperative pirfenidone treatment for lung cancer patients with idiopathic pulmonary fibrosis. Surg Today. 2020;50:469–474. doi:10.1007/s00595-019-01923-5.

32. Fujiwara A, Shintani Y, Funaki S, Kawamura T, Kimura T, Minami M, Okumura M. Pirfenidone plays a biphasic role in inhibition of epithelial-mesenchymal transition in non-small cell lung cancer. Lung Cancer. 2017;106:8–16. doi:10.1016/j.lungcan.2017.01.006.

33. Kozono S, Ohuchida K, Eguchi D, Ikenaga N, Fujiwara K, Cui L, Mizumoto K, Tanaka M. Pirfenidone inhibits pancreatic cancer desmoplasia by regulating stellate cells. Cancer Res. 2013;73:2345–2356.

34. Ishii K, Sasaki T, Iguchi K, Kato M, Kanda H, Hirokawa Y, Arima K, Watanabe M, Sugimura Y. Pirfenidone, an anti-fibrotic drug, suppresses the growth of human prostate cancer cells by inducing g1 cell cycle arrest. J Clin Med. 2019;8(1):44. doi:10.3390/jcm8010044.

35. Zou WJ, Huang Z, Jiang TP, Shen Y-P, Zhao A-S, Zhou S, Zhang S. Pirfenidone inhibits proliferation and promotes apoptosis of hepatocellular carcinoma cells by inhibiting the wnt/beta-catenin signaling pathway. Med Sci Monit. 2017;23:6107–6113. doi:10.12659/MSM.907891.

36. Kramer M, Markart P, Drakopanagiotakis F, Mamazhakypov A, Schaefer L, Didiasova M, Wygrecka M. Pirfenidone inhibits motility of NSCLC cells by interfering with the urokinase system. Cell Signal. 2020;65:109432. doi:10.1016/j.cellsig.2019.109432.

37. Li C, Rezov V, Joensuu E, Vartiainen V, Rönty M, Yin M, Myllärniemi M, Koli K. Pirfenidone decreases mesothelioma cell proliferation and migration via inhibition of ERK and AKT and regulates mesothelioma tumor microenvironment in vivo. Sci Rep. 2018;8(1):10070. doi:10.1038/s41598-018-28297-x.

38. Mediavilla-Varela M, Boateng K, Noyes D, Antonia SJ. The anti-fibrotic agent pirfenidone synergizes with cisplatin in killing tumor cells and cancer-associated fibroblasts. BMC Cancer. 2016;16(1):176. doi:10.1186/s12885-016-2162-z.

39. Akhurst RJ. Targeting TGF-beta signaling for therapeutic gain. Cold Spring Harb Perspect Biol. 2017;9(10):a022301. doi:10.1101/cshperspect.a022301.

40. Dadrich M, Nicolay NH, Flechsig P, Bickelhaupt S, Hoeltgen L, Roeder F, Hauser K, Tietz A, Jenne J, Lopez R, et al. Combined inhibition of TGFβ and PDGF signaling attenuates radiation-induced pulmonary fibrosis. Oncoimmunology. 2016;5(5):e1123366. doi:10.1080/2162402X.2015.1123366.

41. Yingling JM, McMillen WT, Yan L, Huang H, Sawyer JS, Graff J, Clawson DK, Britt KS, Anderson BD, Beight DW, et al. Preclinical assessment of galunisertib (LY2157299 monohydrate), a first-in-class transforming growth factor-beta receptor type I inhibitor. Oncotarget. 2018;9:6659–6677. doi:10.18632/oncotarget.23795.

42. Reagan-Shaw S, Nihal M, Ahmad N. Ahmad N: dose translation from animal to human studies revisited. Faseb J. 2008;22 (3):659–661. doi:10.1096/fj.07-9574LSF.